ATO Nanoparticles as Support for Reduction and Evolution Oxygen Reactions in PEM Electrolysers

V. Ávila -Vázquez[1], C. Guzmán-Martínez[1], M. Galván-Valencia[1], V. H. Collins-Martínez[2], S. M. Durón-Torres[1].

[1]Universidad Autónoma de Zacatecas, U. A. Ciencias Químicas, Km 6 Carr. Zac-Guad, Ejido la Escondida, C.P. 98160, Zacatecas, Zac. México.
[2] Centro de Investigación en Materiales Avanzados, S.C. Dpto. de Materiales Nanoestructurados, Miguel de Cervantes 120, Complejo Industrial Chihuahua, Chihuahua, C.P. 31190
*Tel: 4929256690 ext. 4655, mail:duronsm@prodigy.net.mx

ABSTRACT

Sb was used as dopant of SnO_2 to prepare a powder of conductive nanoparticles with the aim to be used as a support for PEM electrolysers and fuel cells, the support were prepared by a chemical coprecipitation method. In this work it is reported the physicochemical characterization and the evaluation of the electrochemical response of antimony doped tin oxide as catalytic supports for ORR and OER. Pt and IrO_2 were used as catalysts in the electrochemical oxygen reactions. The ATO was characterized by X-ray Diffraction (XRD), High Resolution Transmission Electron Microscopy (HRTEM) and Energy Dispersive Spectrometry (EDS) techniques. The resistivity of SnO_2 Sb doped conductive nanoparticles was measured by using a Milliohmeter,The electrochemical properties respect to the oxygen reactions were obtained by using CV, LV, RDE, EIS and chronoamperometry techniques. The material obtained presented nanoparticles sizes of 6-8 nm and the electrochemical results indicate that ATO nanoparticles synthesized could be used as support in electrolysers and fuel cells.

*Keywords:*ATO, OER, Coprecipitation

1. INTRODUCTION

The direct chemical-electrical energy conversion processes in fuel cells (FC) with high efficiency and low pollutant emission is a well known fact and different FC systems are currently under study. Platinum or platinum-based catalysts highly dispersed on a conductive support are commonly used as cathodic electrode materials in low temperature FC. By the other side, water electrolysers (WE) are recognized as electrochemical devices for hydrogen production that require materials (catalysts and supports) with good features to carry out the reactions. In this case, supported oxide catalyst as IrO_2 or RuO_2 are used for the oxygen reaction. An ideal support should offer the following properties: (i) good electrical conductivity, (ii) good catalyst–support interaction, (iii) large surface area, (iv) mesoporous structure enabling the ionomer and polymer electrolyte to bring the catalyst nanoparticles close to the reactants and maximize the triple-phase boundary (TPB), (v) good water handling capability to avoid flooding, (vi) good corrosion resistance, and (vii) easy recovery of the catalyst[1, 2]. A good interaction between the catalyst and the support not only improves catalyst efficiency and decreases catalyst loss but also governs charge transfer. The support can also assist in sufficiently enhancing the catalyst performance and durability by reducing catalyst poisoning (e.g. CO, S, etc.); and in some cases it affects the catalyst particle size. Among non-carbonaceous based materials, titania, indium oxide, alumina, silica, tungsten oxide nanostructures and conducting polymers have been widely investigated with the aim to improve the issue of carbon corrosion, which is suffered by all carbon supports [1-3].

Tin dioxide, SnO_2, belongs to the family of transition-metal dioxide compounds with rutile structures. The mineral form of SnO_2 is called cassiterite, and this is the main ore of tin. SnO_2 is usually regarded as an oxygen-deficient n-type semiconductor. Hydrous forms of SnO_2 have been described in the past as stannic acids, although such materials appear to be hydrated particles of SnO_2 [4, 5]. This oxide has been proposed as a support material for fuel cell and electroyser electrocatalysts because of its chemical properties For its use as an electrocatalytic catalyst support, however, the electrical conductance of SnO_2 has to be improved. Tin dioxide has a wide bandgap semiconductor (Eg~3.6 eV) with electrical resistivity varying from 10 to 10^6 Ω cm, depending on the temperature and the stoichiometry of the oxide[6, 7] and doping is needed to increase its intrinsic conductivity. Antimony is one of the most common n-type dopant for SnO_2 used to modify the oxide band structure[8-12]. The SnO_2 modified with Sb (ATO) presents high resistance to corrosion in acid media and because is doped withconductivespeciesasSb^{5+} or Sb^{3+},its electrical conductivity reaches values of 10^2or $10^3\Omega^{-1}$ cm^{-1}[13-15].Several studies indicate that ATO could be used as catalyst support for OER and ORR in water electrolizer (WE) and FCs, being reported an improvement in the stability of the support as compared with a nundoped oxide, at the conditions of oxygen evolution[12, 13, 16-22].

According to previous reports, ATO powders have been mainly synthesized by different procedures: sol–gel, hydrothermal preparation, coprecipitation , thermal evaporation , polymer pyrolysis and solid-state reaction. Compared to other methods, coprecipitation from homogeneous solutions containing metallic sources is a cost-efficient method of ATO synthesis, which presents many advantages like high purity, small crystalline size, short preparation time, low cost and large scale production. Thus, it is recognized as the best method for commercial production of ATO powders [8, 9, 23-28].

This paper presents the results of the study of the OER and ORR kinetics of IrO_2 an Pt catalyst supported on ATO synthesized by co-precipitation with a heat treatment time of 1h. X-ray Diffraction (XRD), High Resolution Transmission Electron Microscopy (HRTEM) and Energy Dispersive Spectrometry (EDS) techniques were employed to characterize the microstructure of ATO. The electrochemical properties respect to the oxygen reactions were obtained by using CV, LV, RDE, EIS and chronoamperometry techniques. The resistivity of SnO_2 Sb doped conductive nanoparticles was measured by using a Milliohmeter system. The ATO support obtained suitable candidate to be used in the reactions of oxygen.

2. EXPERIMENTAL SECTION

2.1 Synthesis of materials.

The IrO_2catalyst for OER was synthesized using a coloidal system that consist in mixing a 0.02M $H_2IrCl_6 \cdot nH_2O$ solution with 1M KOH for 50 min at a temperature near to 100 °C. The dark iridium hidroxide precursor obtained was then annealed at 400°C for 1 h [29-34]. ATO supports were obtained by a co-precipitation method from the reaction between $SnCl_4.5H_2O$ and $SbCl_3$ (StremChem) precursors in hidrochloric acid medium at moderate temperature (50 °C) for 1 h, the precipitate was dried at 90°C for 24 h, followed by an annealing procedure at 500 °C and heat treatment time of 1h[35-38].

2.2 Electrodes preparation

The electrodes were prepared from a catalytic ink comprising of 90µL of Nafion® (5wt. %, Aldrich), 540 µL of ethanol spectroscopic grade, 6mg of IrO_2 or Pt as catalyst and 6 mg of ATO or vulcan as support. The ink was obtained using a FRITSCH/PULVERISETTE 23 mini-mill for a period of 0.5h in order to homogenize the mixture and promote dispersion of the ink. Later, the resulting suspensions were hold in an ultrasonic bath for 0.5 h with the aim of gain additional dispersion of the mixture. Subsequently, a volume of each ink was deposited on a clean polished glassy carbon disk electrode (GCE) (A = 0.07068 cm^2). The coated GCEs were dried in a furnace at 80°C for 10 min. IrO_2 and Pt films supported on ATO or vulcan were used as working electrodes for the OER and ORR kinetic studies. All the current values reported in this paper are normalized to the electrode geometric area.

2.3 Electrochemical characterization of electrodes

All the experiments were performed in a double-compartment electrochemical glass cell. An Hg/Hg_2SO_4/0.5 M H_2SO_4 (ESM = 0.69V vs. NHE) electrode was used as reference which was positioned as close to the working electrode as possible by means of a Luggin capillary. A Pt-mesh was used as counter-electrode and the aqueous electrolytic medium was 0.5 M H_2SO_4 at room temperature. The electrochemical measurements were performed using an EG&G PAR VersaSTAT 3 Potentiostat/Galvanostat. In this study, all measured values of potential are reported respect to the normal hydrogen electrode (NHE).

Cyclic voltammetry (CV) was carried out to evaluate the effect of different ATO in the IrO_2 or Pt electrodes by scanning the potential at a rate of 50 mV s^{-1} between -0.16 V and 1.54 V under a N_2 atmosphere. Oxygen evolution experiments were performed by linear scan voltammetry (LSV) at a scan rate of 5 mV s^{-1} in the anodic direction from 0.59 V to 1.69 V in O_2-free electrolyte solution at a constant electrode rotation frequency of 1000 rpm. The rotation rate was controlled by a PINE MSRX precision rotating system.

In addition, electrochemical impedance spectroscopy (EIS) experiments were carried out in the potentiostatic mode in the 100 kHz to 10 mHz frequency range. The impedance spectra were registered with a logarithmic data collection scheme at 10 steps per decade at 1.67 V of potential with an alternate signal amplitude of 10 mV.

3. **RESULTS AND DISCUSSION**

3.1 **Physicochemical Characterization**

The XRD diffraction patterns of ATO are shown in Figure 1, here the characteristic peaks of SnO_2 with a cassiterite tetragonal stucture and a rutile phase can be observed. Due to the minimal dopant quantity used, any diffraction peak related with Sb could be identified. The two diffractograms shown correspond to samples obtained from annealing times of 1h (black) and 3h (red) respectively. A SnO signal peak has been identified at 29 degrees in the red diffractogram.

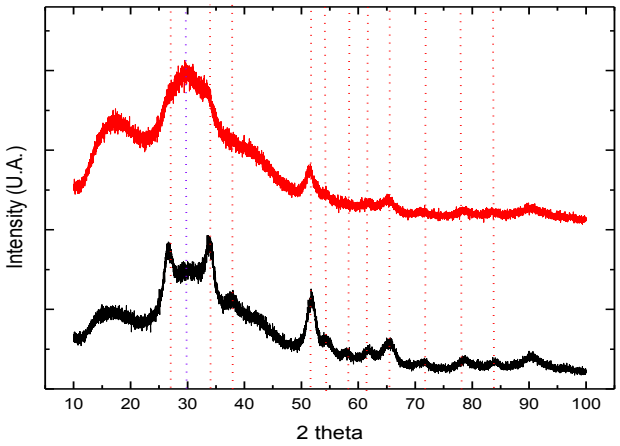

Figure 1. X-ray diffraction patterns of ATO obtained at 500 °C.

Figure 2 a) shows the SEM micrograph of 4 wt% antimony-doped tin oxide nanoparticle of ATO. The surface morphology of ATO powder showed the presence of spherical-shaped particles of 60-70nm composed by the

agglomeration of smaller crystallites. An ATO TEM micrograph is shown in Figure 2 b), homogeneous particles with sizes ranging from 5 to 7 nm can be clearly observed. The particles were nanocrystalline in nature with an estimated average size of 6 nm such as shown in histogram of Figure 2 c), which indicates that the nanoparticles should be monocrystalline. [37, 39-41]. These sizes are smaller than the average value of 20 to 7 nm reported for commercial ATO [15, 42].

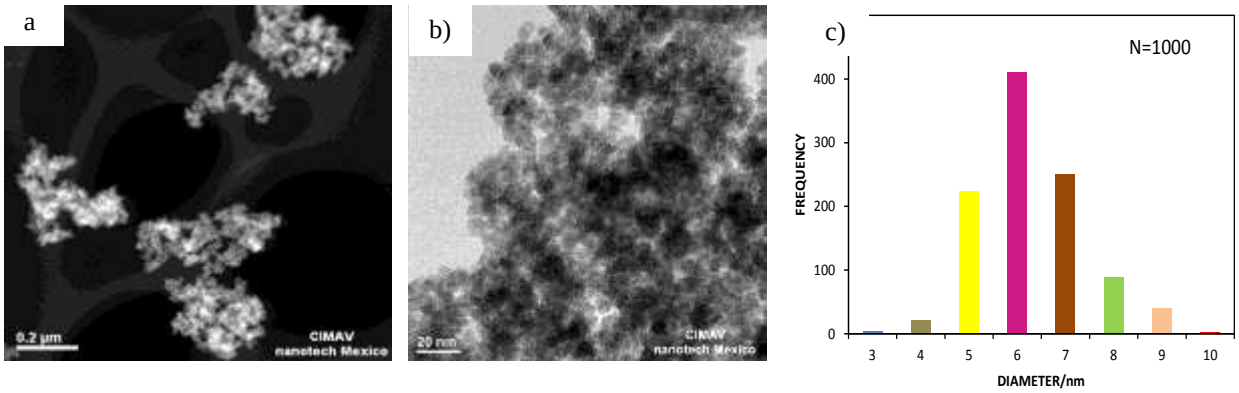

Figure 2. SEM micrograph of ATO powder a), TEM micrograph b), histogram of the particle size average of ATO.

Figure 3 shows HR-TEM and a typical electron diffraction pattern of ATO 1h nanocrystalline grain. The electron diffraction (ED) rings can be indexed to the pattern of ATO with cassiterite structure. The small size ATO particles is responsible for the somewhat thicker diffraction circles in Figure 3 b). The typical lattice parameters of SnO_2 are changed when Sn ions were replaced by Sb ions. The ionic radius of Sn^{4+}, Sb^{5+} and Sb^{3+} is 0.72, 0.62 and 0.90 Å respectively. When Sb^{5+} enters the SnO_2 lattice, the lattice parameters became therefore smaller, contrarily if Sb^{3+} ions increase the lattice parameters [9,10, 23, 43].

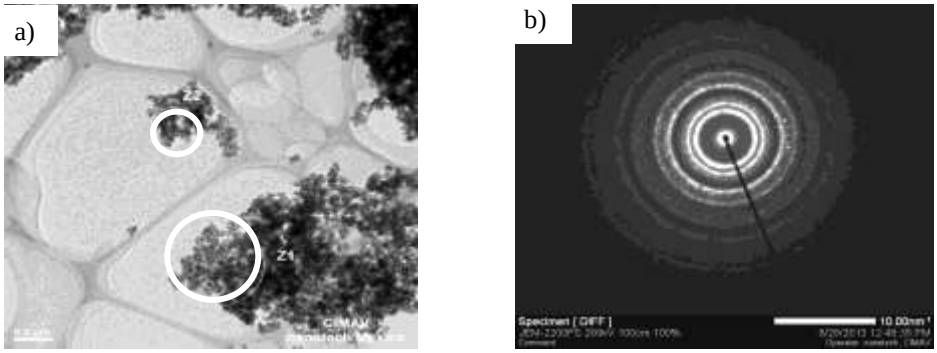

Figure. 3 HR- TEM micrographs of ATO a) and the corresponding electron diffraction patterns (right) b).

As obtained from the high-resolution fringes of synthesized ATO (Figure 4), the particles were composed of regularly ordered crystallites with a lattice distance of 3.34 $\dot{A}$ corresponding to the (d 110) inter- planar spacing, this value was slightly smaller that 3.458 $\dot{A}$, wich correspond to the standard lattice spacing of SnO_2 sample (JCPDS PDF# 41-1445).This result confirms the formation of tetragonal crystal structure of Sb-doped SnO_2[43, 44].

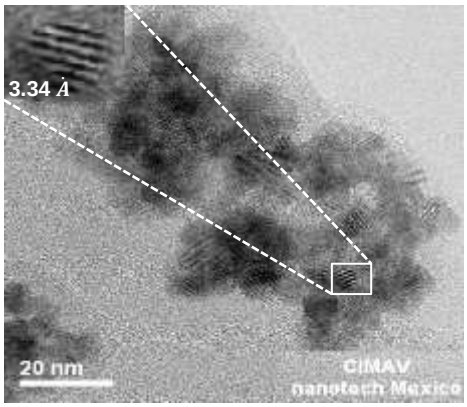

Figure 4. HR-TEM image of ATO.

Figures 5 b) and c) show the Sn and Sb abundance histograms obtained from EDS spectrum of ATO in a particular area correspondig to the linear scanning of sample showed in micrograph 5 a). The metallic element contents in the EDS spectra of different sample regions are shown in Table 1.Theoretically for synthesis was placed a 16% weight of dopant corresponding to a theoretical atomic ratio of Sn: Sb of 6:1, however, the EDS analysis indicates that only between 2% and 4% in weight of dopant is present in the final material.

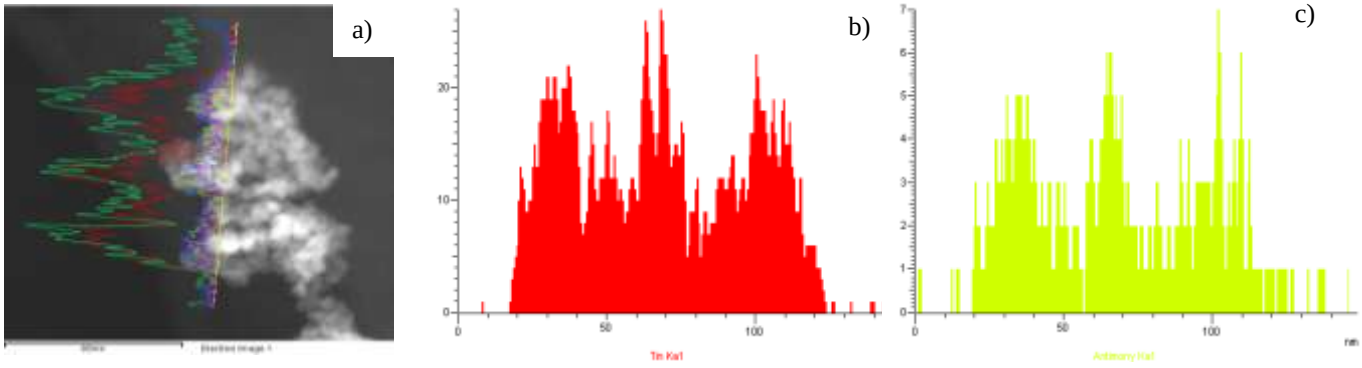

Figure. 5 EDS elements abundance histograms of ATO, Sn (red), Sb (green).

Table 1 EDS concentration of Sn and Sb for ATO synthesized.

	ATO			
Spectrum	Sn % weight	Sb % weight	% Sn atomic	% Sb atomic
Spectrum 1	82.16	4.56	70.44	3.81
Spectrum 2	78.26	2.39	62.4	1.86
Spectrum 3	76.63	6.92	63.3	5.58
Max.	82.16	6.92	72.36	5.94
Min.	76.63	2.39	59.87	1.82

3.2 Electrochemical characterization

3.2.1 Evaluation of the supports by cyclic voltammetry

Previous studies on the relationship between annealing time and the electrochemical performance ATO shown that less time heat treatment presented best performance[16, 45]. The Figure 6 shows typical cyclic voltammograms a) and linear scan voltammograms b), obtained for IrO_2 supported on ATO 1h and 3h in N_2 saturated 0.5 M H_2SO_4 solution. The CV diagrams reveal that the electrochemical response for IrO_2 is practically unchanged with the use of different ATO supports, the current density (j) attributed to IrO_2 supported on ATOs may be considered an evidence that the dispersion of IrO_2 is improved with the use of this supports. The off-peak potential for oxygen evolution on all the IrO_2/ATO electrodes appears near to 1.5 V, this response is more clearly defined in the linear voltammograms showed in Figure 6 b).

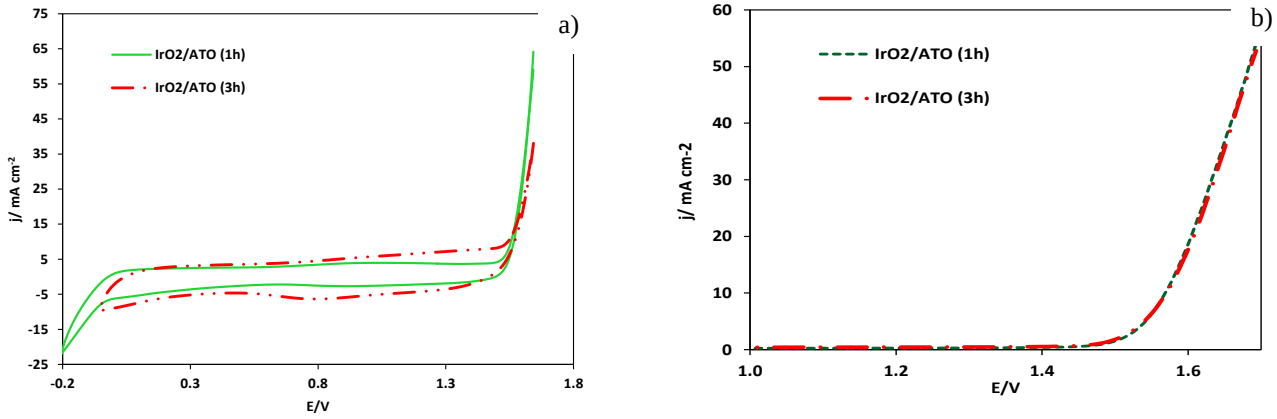

Figure 6. Cyclic voltammogram a) and linear scan voltammetry b) of GCEs coated with IrO_2/ATO in N2 saturated 0.5 M H_2SO_4 at 50 mV s^{-1}. 50 wt % IrO_2/ATO: and room temperature.

The suitable electrochemical behavior of ATO as support for OER is already known [12, 15, 35, 38, 45, 46]. The trends in the development of supports and catalysts is to optimize the synthesis for the preparation of such materials, in this context, it is intended that these materials can be used interchangeably in the OER and ORR, where main application may be in the development of URFC, for this reason in this work also was developed a study with the aim to probe the electrochemical activity of mixtures of ATO based supports and catalysts in the both reactions of oxygen.

For this study was utilized Vulcan and ATO for the mixtures as support and Pt and IrO_2 as catalysts. The proportions used are described in Table 2.

Table 2. Proportion used by inks in mixed support study.

Item	Catalysts		Support	
	% weight Pt	% weight IrO_2	% weight Vulcan	% weight ATO
1	-	100	75	25
2	-	100	25	75
3	100	-	75	25
4	100	-	25	75
5	100	-	50	50
6	-	100	50	50
7	50	50	50	50

The Figure 7 compares the cyclic voltammograms obtainedfor Pt a) and IrO_2 b) supported on vulcan and ATO in N_2 saturated 0.5 M H_2SO_4 solution. The voltammograms of Pt a) supported on mixture support shows that the reactions associated with the surface of Pt in an acid medium are limited by the support especially when the vulcan was in a smaller proportion avoiding identify the characteristic peaks of Pt on a clearly way, nevertheless the general electrochemical behavior in acid medium of platinum is still outlined in the voltammogram. The voltammograms corresponding to IrO_2 catalyst, Figure b), show broad waves corresponding to the redox reactions over the Ir surface, these waves are more evident when Vulcan is in a higher proportion in the support. In the voltammograms of Figure. 7 a) also can also be observed that the potential onset for oxygen evolution in the Pt/ATO electrode appears near to 1.7 V, while the corresponding oxygen evolution peaks of IrO_2/mixed supports electrodes (Figure. 7 b)) appear about 300 mV less positive potential values.

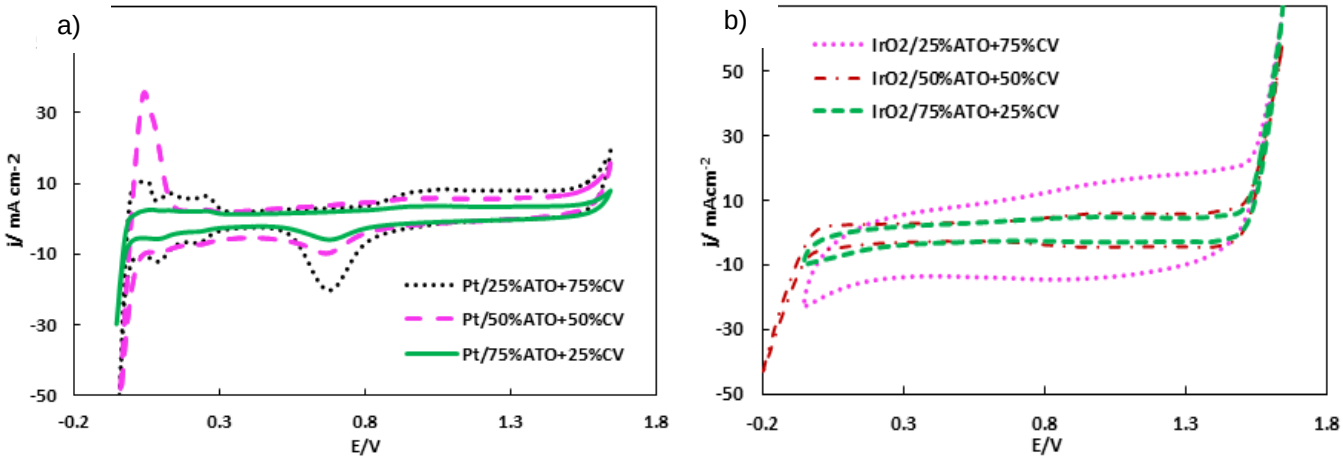

Figure 7. Cyclic voltammograms of Pt a) and IrO_2b) supports on mixtures of vulcan and ATOin N_2satured0.5 M H_2SO_4 at 50 mV s^{-1}.

The Figure 8 shows the RDE diagram a) with typical diagram j–V for ORR at a constant rotating speed of RDE, the difference in the limiting currents for different mixed supports may be attributed to the surface coverage of the catalyst and the physical properties such as the porosity of the catalyst and nature the supports deposited on the glassy carbon electrode. The ORR curves show the classical mixed, kinetic and diffusion control zones, although these regions are better defined when the vulcan is in a greater proportion. On the other hand the Figure 8 b) shows the linear scan voltammograms for OER with IrO_2 t on different mixtured supports, the voltammograms practically

remain unchanged with the use of mixtues, the OER begins in a potential near to 1.54 V, although can observe a higher current densities are obtained when higer ATO proportions are used in the mixed support.

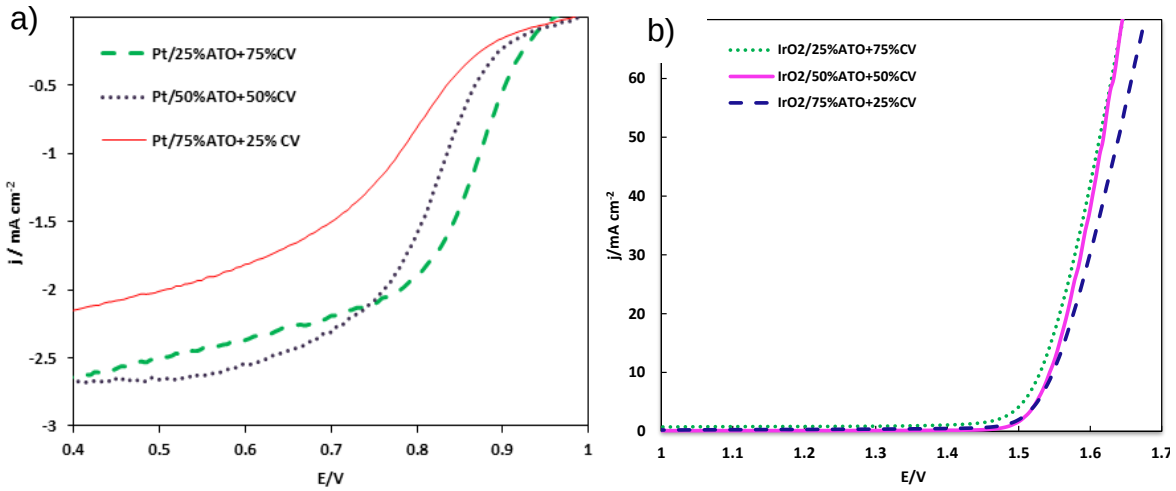

Figure 8. RDE for ORR of Pt support on mixture support in O_2 satured a) and linear scan voltammograms for OER of IrO2in N_2 saturedb), in solution 0.5 M H_2SO_4, at v=5 mVs^{-1}.

EIS measurements for both oxygen reactions was carried out on Pt and IrO_2 on mixed supports in 0.5 M H_2SO_4 solution, in the potensiostatic mode at an anodic potential of 1.67V for OER and 0.8V for ORR. Figure 9 a) shows the Nyquist plots for ORR, it can be observed that the reaction is faster when the Pt is supported on a mixed support with 50:50 % weight ratio, followed by the support of proportion 25% weight of ATO. A similar behavior occurs for the OER, in this case the suport of proportion 75% weight in vulcan is better for OER as can be seen by the smaller semicircle in the complex impedance plane, however the lesser stability and the corrosion problems that carbon presents at the OER potentials, means an opportunity of use of 50:50 % weight support mixture in this reaction. The R_{ct} and R_S values obtained from Non-Linear Square Adjustment of EIS data for the oxygen reactions are shown in Table 2.

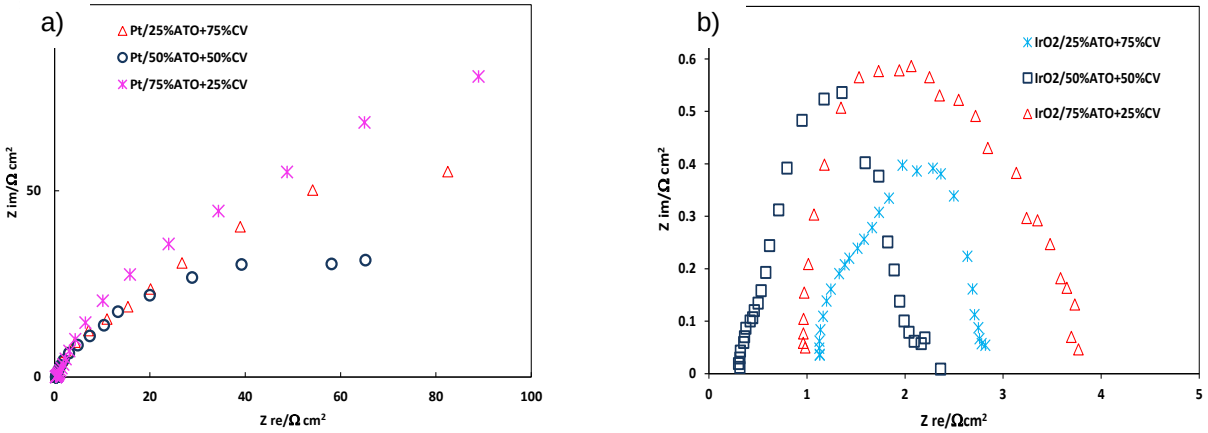

Figure 9. Nyquist plots for ORR and OER on Pt and IrO_2 support on mixtures at anodic potential value of 0.8 and 1.57 V respectively, in O_2-free 0.5 M H_2SO_4 solutions.

Table 2. R_{ct} and R_S values obtained of EIS for OER and ORR with mixtures support.

	Proportion of catalyst/support	Rs / Ω cm^2	Rct / Ω cm^2
RRO (0.8V)	Pt/75%ATO+25%CV	6.6	151.8
	Pt/50%ATO+50%CV	1.32	110.5
	Pt/25%ATO+75%CV	5.3	506.2
REO (1.67 V)	IrO_2/75%ATO+25%CV	1.1	2.6
	IrO_2/50%ATO+50%CV	0.5	2.4
	IrO_2/25%ATO+75%CV	1.3	1.5

Figure 10 shown the electrochemical stability for the OER, The chronoamperograms shown, were obtained at a potential of 1.63V vs. ENH for 8 h. Can be observed that the IrO_2 support on proportion 50:50 % weight of Vulcan and ATO presents more stability for OER since virtually no significant current loss is obtained during the test period, while in the rest of the proportions a slight loss of the current density can be observed, this results suggests that the proportion of 50:50 % weight may be a promising option of support to perform the OER.

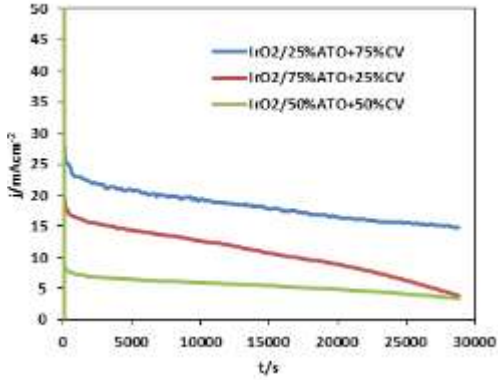

Figure 10.Chronoamperograms of IrO_2 on mixtures of supports for OER in 0.5 M H_2SO_4 at 1.63 V and room temperature.

Finally, the consecutive cyclic performance respect to the EOR and ORR was evaluated using the mixed Pt and IrO2 catalysts and mixed ATO and CV supports proportions described in the item 7 of Table 1. The Figure 11 shows the RDE and LSV plots obtained from 100 sequential experiments between ORR and OER. The Figure 11 a) shows the RDE plots for ORR obtained with rotation and b) without rotation from the first to the 100th measurement (in aim of simplicity only four curves of the series are presented). It can be observed in Figure 11 b) that the absence of rotation does not allow a clear formation of kinetic, diffusional and mixed control zones in the voltammograms. However in the case the LSV was observed that the rotation could be causing physical perfidious of the film deposited on the electrode Figure 11 c), and a loss of lower current density when not rotation Figure 11 d).

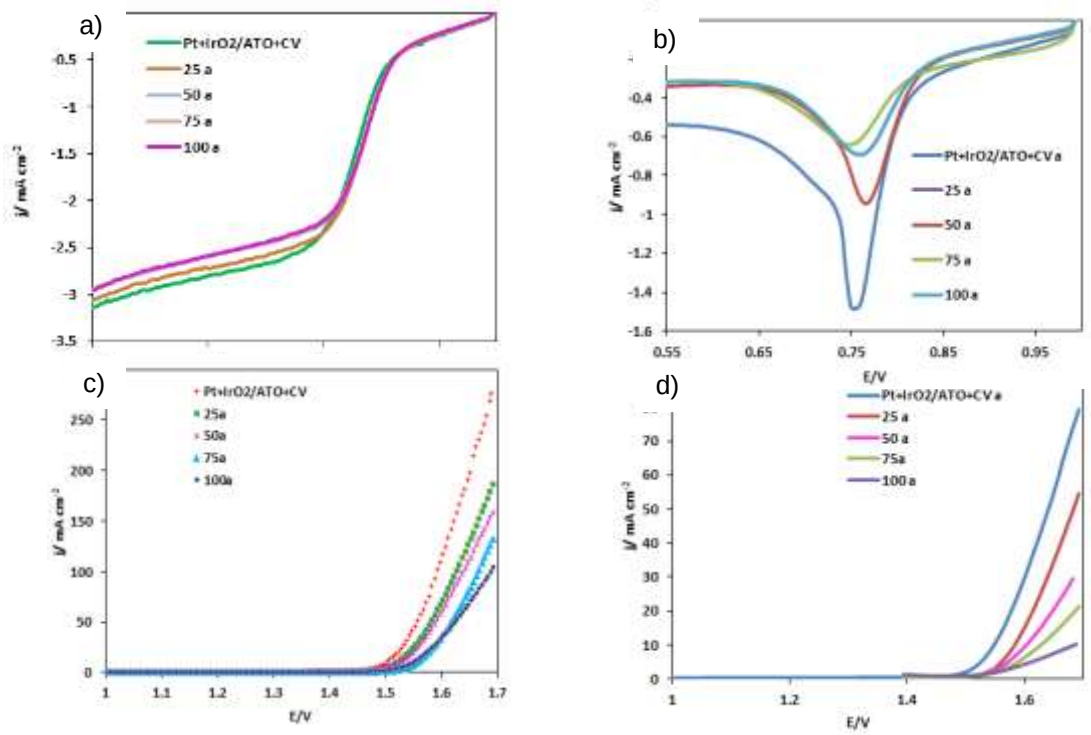

Figure 11. RDE for ORR with rotation a) no rotation b) and LSV with rotation c) no rotation d) of catalyst and support mixture electrodes in O_2 satured (for RDE), in N_2 satured (for LSV)0.5 M H_2SO_4, at v=5 mVs^{-1}.

4. CONCLUSIONS

ATO was obtained with characteristics of a suitable support for IrO_2 used as catalyst the present sufficient catalytic activity for OER, the parameters that have the greatest impact on performance Electrochemical bracket are pH and the time of calcining, being neutral pH calcined short times (1 and 3 h) the most suitable conditions for the synthesis.

The ATO calcined for 1 h showed particle sizes between 5-7 nm , quasi-spherical shape and a homogeneous distribution into small 60-70 nm agglomerates. Furthermore ATO presented calcined for 3 h similar particles with sizes between 7 and 10 nm, grouped in small agglomerates of 200 to 300 nm. The comparison of ATO + vulcan mixture was determined that mixtures ATO 25 +75%vulcan weight and 50 % ATO +50% vulcan are those that can be used indistinctly in the ORR and OER. Studies to the mixture of Pt + IrO_2/ATO+ vulcan with and no rotation showed promising results for OER give greater electrochemical stability when the experiments were carried no rotation. The ORR is not significantly altered with various catalyst / support mixtures

.

5. ACKNOWLEDGMENTS

The authors wish to thank the mexican CONACyT (Project 167012) for financial support of this work.

6. REFERENCES

1. Antolini, E., Composite materials: An emerging class of fuel cell catalyst supports. Applied Catalysis B: Environmental, 2010. 100(3–4): p. 413-426.
2. Sharma, S. and B.G. Pollet, Support materials for PEMFC and DMFC electrocatalysts—A review. Journal of Power Sources, 2012. 208(0): p. 96-119.
3. Long, N.V., et al., The development of mixture, alloy, and core-shell nanocatalysts with nanomaterial supports for energy conversion in low-temperature fuel cells. Nano Energy, 2013. 2(5): p. 636-676.
4. Oviedo, J. and M.J. Gillan, Energetics and structure of stoichiometric SnO2 surfaces studied by first-principles calculations. Surface Science, 2000. 463(2): p. 93-101.
5. Rajendran, V. and K. Anandan, Size, morphology and optical properties of SnO2 nanoparticles synthesized by facile surfactant-assisted solvothermal processing. Materials Science in Semiconductor Processing, 2012. 15(4): p. 393-400.
6. Antolini, E. and E.R. Gonzalez, Ceramic materials as supports for low-temperature fuel cell catalysts. Solid State Ionics, 2009. 180(9–10): p. 746-763.
7. Zhang, D., et al., Surface morphologies and properties of pure and antimony-doped tin oxide films derived by sol–gel dip-coating processing. Materials Chemistry and Physics, 2006. 100(2–3): p. 275-280.
8. Lu, H.F., et al., Preparation of ATO nanorods and electrical resistivity analysis. Materials Letters, 2012. 68(0): p. 237-239.
9. Krishnakumar, T., et al., Structural, optical and electrical characterization of antimony-substituted tin oxide nanoparticles. Journal of Physics and Chemistry of Solids, 2009. 70(6): p. 993-999.
10. Hu, P., H. Yang, and J. Ouyang, Synthesis and characterization of Sb–SnO2/kaolinites nanoparticles. Applied Clay Science, 2012. 55(0): p. 151-157.
11. Hu, Y., H. Zhang, and H. Yang, Synthesis and electrical property of antimony-doped tin oxide powders with barite matrix. Journal of Alloys and Compounds, 2008. 453(1–2): p. 292-297.
12. Xu, J., et al., Antimony doped tin oxides and their composites with tin pyrophosphates as catalyst supports for oxygen evolution reaction in proton exchange membrane water electrolysis. International Journal of Hydrogen Energy, 2012. 37(24): p. 18629-18640.
13. Wang, L.S., et al., Synthesis and electrical resistivity analysis of ATO-coated talc. Powder Technology, 2012. 224(0): p. 124-128.
14. Zhukova, A.A., et al., Influence of antimony doping on structure and conductivity of tin oxide whiskers. Thin Solid Films, 2009. 518(4): p. 1359-1362.
15. Marshall, A.T. and R.G. Haverkamp, Electrocatalytic activity of IrO2–RuO2 supported on Sb-doped SnO2 nanoparticles. Electrochimica Acta, 2010. 55(6): p. 1978-1984.
16. Cruz, J.C., et al., Synthesis and evaluation of ATO as a support for Pt–IrO2 in a unitized regenerative fuel cell. International Journal of Hydrogen Energy, 2012. 37(18): p. 13522-13528.
17. Jung, D.-W. and D.-W. Park, Synthesis of nano-sized antimony-doped tin oxide (ATO) particles using a DC arc plasma jet. Applied Surface Science, 2009. 255(10): p. 5409-5413.
18. Kim, D.-W., et al., Preparation of hard agglomerates free and weakly agglomerated antimony doped tin oxide (ATO) nanoparticles by coprecipitation reaction in methanol reaction medium. Materials Chemistry and Physics, 2006. 97(2–3): p. 452-457.
19. Wu, X. and K. Scott, RuO2 supported on Sb-doped SnO2 nanoparticles for polymer electrolyte membrane water electrolysers. International Journal of Hydrogen Energy, 2011. 36(10): p. 5806-5810.
20. Gurrola, M.P., et al., High surface electrochemical support based on Sb-doped SnO2. Journal of Power Sources, 2013. 243(0): p. 826-830.
21. Pan, C., et al., Platinum–antimony doped tin oxide nanoparticles supported on carbon black as anode catalysts for direct methanol fuel cells. Journal of Power Sources, 2011. 196(15): p. 6228-6231.
22. You, D.J., et al., Platinum–antimony tin oxide nanoparticle as cathode catalyst for direct methanol fuel cell. Catalysis Today, 2009. 146(1–2): p. 15-19.
23. Sladkevich, S., et al., Antimony doped tin oxide coating of muscovite clays by the Pechini route. Thin Solid Films, 2011. 520(1): p. 152-158.
24. Liu, T.J., et al., Conducting antimony-doped tin oxide films derived from stannous oxalate by aqueous sol–gel method. Applied Surface Science, 2008. 254(20): p. 6547-6553.
25. Zhang, D., et al., Microstructure and electrical properties of antimony-doped tin oxide thin film deposited by sol–gel process. Materials Chemistry and Physics, 2006. 98(2–3): p. 353-357.
26. Benrabah, B., et al., Impedance studies of Sb doped SnO2 thin film prepared by sol gel process. Superlattices and Microstructures, 2011. 50(6): p. 591-600.
27. Yang, F., et al., Preparation of Highly Dispersed Antimony-doped Tin Oxide Nano-powder via Ion-exchange Hydrolysis of SnCl4 and SbCl3 and Azeotropic Drying. Chinese Journal of Aeronautics, 2007. 20(2): p. 181-186.

28. Yang, F., et al., Preparation of highly dispersed antimony-doped tin oxide nanopowders by azeotropic drying with isoamyl acetate. Transactions of Nonferrous Metals Society of China, 2007. 17(3): p. 626-632.
29. Cruz, J.C., et al., Nanosized Pt/IrO2 electrocatalyst prepared by modified polyol method for application as dual function oxygen electrode in unitized regenerative fuel cells. International Journal of Hydrogen Energy, 2012. 37(7): p. 5508-5517.
30. Siracusano, S., et al., Electrochemical characterization of single cell and short stack PEM electrolyzers based on a nanosized IrO2 anode electrocatalyst. International Journal of Hydrogen Energy, 2010. 35(11): p. 5558-5568.
31. Vazquez-Gomez, L., S. Ferro, and A. De Battisti, Preparation and characterization of RuO2–IrO2–SnO2 ternary mixtures for advanced electrochemical technology. Applied Catalysis B: Environmental, 2006. 67(1–2): p. 34-40.
32. Zhang, Y., et al., Deposited RuO2–IrO2/Pt electrocatalyst for the regenerative fuel cell. International Journal of Hydrogen Energy, 2007. 32(3): p. 400-404.
33. Mayousse, E., et al., Synthesis and characterization of electrocatalysts for the oxygen evolution in PEM water electrolysis. International Journal of Hydrogen Energy, 2011. 36(17): p. 10474-10481.
34. Papazisi, K.M., et al., Preparation and characterization of IrxPt1−xO2 anode electrocatalysts for the oxygen evolution reaction. International Journal of Hydrogen Energy, 2012. 37(21): p. 16642-16648.
35. Huaming, Y.P.H., Controlled coating of antimony-doped tin oxide nanoparticles on kaolinite particles. Applied Clay Science, 2010. 48(3): p. 368-374.
36. Yang, H., Y. Hu, and G. Qiu, Preparation of antimony-doped SnO2 nanocrystallites. Materials Research Bulletin, 2002. 37(15): p. 2453-2458.
37. Zheng, M. and B. Wang, One-step synthesis of antimony-doped tin dioxide nanocrystallites and their property. Transactions of Nonferrous Metals Society of China, 2009. 19(2): p. 404-409.
38. Xiaozhen, L., et al., Complexation-Coprecipitation Synthesis and Characterization of Erbium and Antimony Doped SnO2 Conductive Nanoparticles. Journal of Rare Earths, 2007. 25, Supplement 1(0): p. 72-76.
39. Bai, F., et al., One-step synthesis of monodispersed antimony-doped tin oxide suspension. Materials Letters, 2006. 60(25–26): p. 3126-3129.
40. Liu, G., et al., Nanosphere-structured composites consisting of Cs-substituted phosphotungstates and antimony doped tin oxides as catalyst supports for proton exchange membrane liquid water electrolysis. International Journal of Hydrogen Energy, 2014. 39(5): p. 1914-1923.
41. Zhang, J. and L. Gao, Synthesis and characterization of antimony-doped tin oxide (ATO) nanoparticles by a new hydrothermal method. Materials Chemistry and Physics, 2004. 87(1): p. 10-13.
42. Gurrola, M.P., et al., Evaluation of the corrosion of Sb-doped SnO2 supports for electrolysis systems. International Journal of Hydrogen Energy, (0).
43. Du, Y., et al., Fabrication and excellent conductive performance of antimony-doped tin oxide-coated diatomite with porous structure. Materials Chemistry and Physics, 2012. 133(2–3): p. 907-912.
44. Chen, X., Synthesis and characterization of ATO/SiO2 nanocomposite coating obtained by sol–gel method. Materials Letters, 2005. 59(10): p. 1239-1242.
45. Manesse, M., et al., Preparation and characterization of antimony-doped SnO2 thin films on gold and silver substrates for electrochemical and surface plasmon resonance studies. Electrochemistry Communications, 2008. 10(7): p. 1041-1043.
46. Yin, M., et al., Highly active and stable Pt electrocatalysts promoted by antimony-doped SnO2 supports for oxygen reduction reactions. Applied Catalysis B: Environmental, 2014. 144(0): p. 112-120.